A fluid inclusion study of blueschist-facies lithologies from the Indus suture zone, Ladakh (India): Implications for the exhumation of the subduction related Sapi-Shergol ophiolitic mélange

A fluid inclusion study of blueschist-facies lithologies from the Indus suture zone, Ladakh (India): Implications for the exhumation of the subduction related Sapi-Shergol ophiolitic mélange

By

Himanshu Kumar Sachan[1*], Aditya Kharya[1], P. Chandra Singh[1], Franco Rolfo[2], Chiara Groppo[2], Sameer Tiwari[1]

1 Wadia Institute of Himalayan Geology, 33 GMS Road, Dehra Dun – 248 001 (India)

2 Department of Earth Sciences, University of Torino, Via Valperga Caluso 35, Torino, 10125, Italy and IGG-CNR, Via Valperga Caluso 35, Torino, 10125, Italy

Corresponding author: *hksachan@wihg.res.in

Abstract

The best occurrence of blueschist-facies lithologies in Himalaya is that of the Shergol Ophiolitic Mélange along the Indus suture zone in Ladakh region of north-western India. These lithologies are characterized by well preserved lawsonite-glaucophane-garnet-quartz assemblages. This paper presents for the first time the results of a detailed fluid inclusion study on these lithologies, in order to understand the fluid P-T evolution and its tectonic implications.

The blueschist rocks from Shergol Ophiolitic Mélange record metamorphic peak conditions at ~ 19 kbar, 470°C. Several types of fluid inclusions are trapped in quartz and garnet, most of them being two-phase at room temperature. Three types of fluid inclusions have been recognised, basing on microtextures and fluid composition: Type-I are primary two-phase carbonic-aqueous fluid inclusions ($V_{CO2} – L_{H2O}$); Type-II are two-phase ($L_{H2O} – V_{H2O}$) aqueous fluid inclusions, either primary (Type–IIa) or secondary (Type–IIb); Type–III are re-equilibrated fluid inclusions. In the Type–I primary carbonic-aqueous inclusions, H_2O is strongly predominant with respect to CO_2; the homogenization temperature of CO_2 range from -7 to -2°C. The clathrate melting temperature in such inclusions varies in between +7.1 to +8.6°C. Type-II two-phase aqueous fluid inclusions show a wide range of salinity, from 7.8–14 wt.% $NaCl_{eq}$ (Type–IIa) to 1.65–6.37 wt.% $NaCl_{eq}$ (Type–IIb) with accuracy ± 0.4wt.% $NaCl_{eq}$.

Type-I and Type-IIa primary fluid inclusions are hosted in peak minerals (garnet and quartz included in garnet), therefore they were likely entrapped at, or near to, peak P-T conditions. The dominantly aqueous fluid of both Type-I and Type-IIa inclusions was most likely produced through metamorphic devolatilization reactions occurring in the subducting slab. Despite their primary nature, the isochores of Type-I and Type-IIa inclusions do not intersect the peak metamorphic conditions of the blueschist mineral assemblage, suggesting that these inclusions stretched or re-equilibrated during nearly isothermal decompression from 19 kbar to 3 kbar or

41 less, at T=290°C. This conclusion is further supported by their large variability in shapes and
42 sizes which range from irregular inclusions ('C'/arc shaped, hook shape and satellite type). This
43 decompression stage was followed by nearly isobaric cooling, testified by the occurrence of
44 dendritic networks of decrepitated and 'imploded' fluid inclusions.
45 Key Words: Fluid inclusions, Blueschist, lawsonite, Ladakh, Himalaya
46

47 **1. Introduction**

48 Fluid inclusions occurring in high pressure – low temperature (HP-LT) metamorphic rocks
49 reveal the nature of fluid as well as the role of fluid in the subduction history of continental or
50 oceanic crust. Fluid inclusions can also be used as a marker point in constraining parts of the
51 *P–T* paths of different metamorphic rocks (e.g. Hollister et al., 1979; Santosh, 1987; Hames et
52 al., 1989; Sisson et al., 1989; Vry and Brown, 1991; Winslow et al., 1994). Additionally,
53 evidences of fluid–rock interactions occurred during blueschist- and eclogite- facies
54 metamorphism can provide significant insights for our understanding of fluid storage and
55 recycling during subduction or continent-continent collision processes (Brunnsman et al., 2000;
56 Scambelluri and Phillipott, 2001).
57 The post-entrapment modification of the size and shape of fluid inclusions in response to
58 deformation, cooling or decompression can help to constrain the P-T paths of their host rocks
59 and hence provide some insights on their exhumation processes (e.g. Scambelluri, 1992;
60 Winslow et al., 1994, Vallis and Scambelluri, 1996; Kuster and Stockhert, 1997; El-Shazly and
61 Sisson, 1999; Bakker and Mamtani, 2000). The detailed observation of the fluid inclusion
62 textures and microthermometric results hold the key to fruitful data elucidation (e.g. Bodnar et
63 al., 1989; Sterner and Bodnar, 1989; Vityk et al., 1994; 1995; Barker, 1995; Sterner et al., 1995;
64 Vityk and Bodnar, 1995; Van den Kerkhof and Hein, 2001).

65 Fluid inclusion studies on subduction-related metamorphic rocks often revealed that the fluid
66 was retained within the subducting slab and that the fluid flow was limited (e.g. El-Shazly and
67 Sisson, 1999; Xiao et al., 2000; Gao and Klemnd, 2001). However, previous fluid inclusion
68 studies focused on HP-LT metamorphic terranes show no general agreement on fluid
69 composition and mechanisms of fluid flow.
70 Blueschists occur in many orogenic belts including the Pacific, Alpine-Himalayan and
71 Precambrian-Phanerozoic belts (Liou et al., 1990). Most of the studies on the blueschist-facies
72 rocks are focused on petrology, mineralogy and geochronology (e.g. Martin et al., 2011; Vitale
73 Brovarone et al., 2011; Chantel et al., 2012; Abers et al., 2013; Cao et al., 2013; Kim et al.,
74 2013; Spandler and Pirard, 2013), whereas the application of fluid inclusion studies to
75 blueschist-facies rocks is limited so far to few examples. Luckscheiter and Morteani (1980)
76 noticed the presence of CO_2-H_2O fluids in glaucophane-bearing rocks from the Tauern
77 Window, while Barr (1990) reported the presence of only aqueous fluid in blueschist rocks
78 from Syros. Invernizzi et al. (1996) studied the fluid inclusions in quartz veins hosted within
79 blueschist-facies rocks, and inferred the re-equilibration history of these fluid inclusions in
80 terms of uplift processes. The re-equilibration of the vast majority of primary fluid inclusions
81 in high *P*-low *T* rocks during exhumation is the main cause for the scarcity of such studies
82 (Touret, 1992). However, Vityk et al. (1994) and Vityk and Bodnar (1995) experimental works
83 on synthetic fluid inclusions presented textural benchmarks for recreating sections of *P*–*T* paths
84 and for enhancing tectonic interpretations.
85 Although the Himalaya is the archetype of collisional orogens, high-pressure metamorphic
86 rocks are rare (e.g. Lombardo and Rolfo, 2000; Guillot et al., 2008). The blueschist-facies rocks
87 in Himalaya are mostly lawsonite-bearing and occur along the Indus Suture Zone in Pakistan
88 (Shangla: Shams, 1972; Frank et al., 1977) and NW India (Sapi–Shergol, Ladakh: Honegger et
89 al., 1989; Groppo et al., 2016; Zildat: Virdi et al., 1977). Few lawsonite- and epidote blueschist-

facies rocks are also reported from the eastern portion of the orogen in the Indo-Burmese Ranges (Nagaland Ophiolite Complex: Ghose and Singh, 1980; Chatterjee and Ghose, 2010; Ao and Bhowmik, 2014). The preservation of lawsonite in the blueschists indicates very low geothermal gradients during subduction as well as during exhumation processes. The best occurrence of such lithologies in the Himalaya is that of Sapi-Shergol: a preliminary petrologic study of these blueschists by Honegger et al. (1989) constrained peak P-T conditions at 9-11 kbar, 350-450°C (conventional thermobarometry). Groppo et al. (2016) estimated significantly higher pressure (19 kbar, 470°C) for the same unit by using *P-T* pseudosection modelling and suggested a very low geothermal gradient (i.e. 8-9°C/km). Sachan and Mukherjee (2001) preliminarily studied the fluids from quartz veins hosted in the blueschist rocks from Sapi-Shergol and provided comments upon their exhumation history. However, these quartz veins are related to a very late stage of the metamorphic evolution, and consequently do not give any direct clue on the blueschist formation and exhumation.

As concerning other subduction-related rocks from the Himalaya, a fluid inclusion study by Mukherjee and Sachan (2009) focusing on the ultra-high pressure eclogites from the Tso Morari, showed the prevalence of high-salinity brine, N_2, CH_4, CO_2 –bearing fluids and low-salinity aqueous fluids. This study shows the complex nature of the fluid involved during deep subduction and exhumation of Indian continental crust. Additionally, Ferrando et al. (2007) reported the presence of pure CO_2 and CO_2-H_2O fluids in granulitized eclogites from eastern Himalaya.

This paper is the first systematic fluid inclusion study on the blueschist rocks from Sapi-Shergol ophiolitic mélange (Ladakh Himalaya, NW India). The fluids associated to peak and retrograde metamorphic stages are characterised, and the source of these fluids is assessed. Moreover, the fluid evolution is discussed in relation to the P–T paths inferred by Groppo et al. (2016) on the base of thermodynamic modelling. The results from this study have important implications for

115 the understanding of the nature and role of fluids during subduction-related metamorphism and
116 the consequent uplift, in the framework of the geodynamic evolution of the Himalayan orogeny.
117

118 ## 2. Geological Setting

119 The blueschists studied in this paper occur along the Indus suture zone in Ladakh, NW India
120 (Fig. 1a). From SE to NW, blueschist-facies lithologies are reported at Zildat, Urtsi, Hinju, and
121 Sapi-Shergol (Honegger et al., 1989). Among these occurrences, the largest one is that of Sapi-
122 Shergol in western Ladakh, south of Kargil. Tectonically, the Sapi–Shergol blueschists belong
123 to a narrow belt and are part of an ophiolitic mélange (Honegger et al., 1989) (Fig. 1b).
124 This ophiolitic mélange is thrusted over the Kargil Molasse to the west as well as to the north,
125 and it is in contact with the Nindam and Lamayuru Formations to the north and to the south,
126 respectively. To the south, the Triassic limestone of the Zanskar Unit is thrusted over the
127 mélange (Frank et al., 1977, Honegger et al., 1982). The ophiolitic mélange is inferred to be a
128 remnant of a paleo-accretionary prism produced by the northward subduction of the Neo-
129 Tethys, originally separating the Ladakh arc to the south from the Asian active margin to the
130 north (Mahéo et al., 2006) (Fig.1a). This paleo-accretionary prism comprises sedimentary
131 bodies including mainly basic lithologies that have been metamorphosed under low-grade to
132 lawsonite blueschist-facies conditions (Frank et al., 1977; Honegger et al., 1989; Reuber et al.,
133 1987; Ahmad et al., 1996; Rolfo et al., 1997; Robertson, 2000; Mahéo et al., 2006). The Sapi–
134 Shergol ophiolitic mélange therefore shows a complex internal architecture, including a number
135 of slivers of the paleo-accretionary prism, intercalated with numerous slivers of other units
136 including the Nindam and Lamayuru Formations, as well as low-grade meta-ophiolitic rocks
137 with serpentinized peridotites intruded by basic dikes (“sheared serpentinites” of Robertson,
138 2000).

The protoliths of the blueschist lithologies cropping out around the Shergol village are mainly basic metavolcanics and volcanoclastites with subordinate amounts of cherts, metasediments and minor carbonatic lithologies. Mahéo et al. (2006) suggested that the blueschists originate from calc-alkaline igneous rocks formed in an intra-oceanic arc environment. Whole-rock and glaucophane K–Ar geochronology gave an age of ca. 100 Ma for the high-pressure metamorphic peak (Honegger et al., 1989). Petrographically, metabasic rocks are mainly fine-grained glaucophane -bearing schists, with lawsonite and minor clinopyroxene and phengite. Metavolcanoclastic rocks show a clastic structure with irregular fragments of metabasic rocks set in a very fine-grained matrix. The clasts generally contain a blue amphibole + lawsonite ± clinopyroxene assemblage. The matrix is very fine-grained and mainly comprises blue amphibole, chlorite and minor aegirine.

Silicic and impure carbonatic metasediments are locally found as intercalations within the metabasic and metavolcanoclastic rocks. The silicic metasediments comprise glaucophane + lawsonite + phengite ± garnet schists, lawsonite + glaucophane + phengite + garnet quartzitic micaschists and glaucophane + garnet + phengite quartzites. Lawsonite and garnet are either fine-grained or porphyroblastic. Lawsonite and garnet porphyroblasts are from few centimeters to few millimeters in size, and generally overgrow the main foliation. The impure carbonatic metasediments are very fine-grained and mainly consist of lawsonite, calcite, glaucophane, and minor phengite ± prehnite.

3. Petrography

A detailed petrographic study of two representative samples of metasediments (samples 14-4B and 14-6F/G) has been carried out. These metapelites are mainly composed of lawsonite, glaucophane, garnet, phengite and quartz, with minor calcite concentrated in late veins.

Accessory minerals are titanite and pyrite. Both samples are very fresh, one of them being relatively fine-grained (sample 14-4B) compared to the other (sample 14-16F/G).

Sample 14-4B is characterised by alternating layers rich in quartz or lawsonite + glaucophane + phengite, respectively (Fig. 2a, b). Glaucophane occurs in both layers as fine-grained idioblasts; it shows characteristic zoning pattern with light blue core and a dark blue rim. The preferred orientation of glaucophane and phengite defines the main foliation. Garnet is weakly zoned and occurs as small idioblasts (Fig. 2b). Lawsonite occurs as fine-grained idioblasts (Fig. 2c); it contains inclusions of quartz and titanite. In the quartz-rich layers, lawsonite locally shows a skeletal habit, being intergrown with quartz.

The main assemblage of sample 14-6F/G is lawsonite + glaucophane + phengite + garnet + quartz, with glaucophane occurring as a major constituent (Fig. 2d). Titanite occurs as accessory mineral. The main foliation, defined by the preferred orientation of glaucophane and minor phengite, is overgrown by lawsonite and garnet porphyroblasts and is locally crenulated (Fig. 2d, e, f). The growth of lawsonite and garnet porphyroblasts pre-dated the crenulation event. Garnet occurs as medium- to coarse-grained idioblasts (Fig. 2e) locally included within the lawsonite porphyroblasts, and shows strong zoning. Variably sized inclusions of glaucophane, actinolite, phengite, quartz, chlorite and rare omphacite are found in garnet porphyroblasts. Glaucophane occurs as fine-grained nematoblasts in the matrix. Porphyroblastic lawsonite is up to 1 centimetre in size and sub-idioblastic, and overgrows the main foliation. Phengite is fine- to medium-grained and is found in association with glaucophane (Fig. 2d). The main foliation is locally crosscut by quartz ± albite ± chlorite veins (Fig. 2f). It is worth noting that in both samples, garnet was predicted to have grown at (or close to) peak P-T conditions, i.e. in the narrow P-T range of 400-470°C, 17-19 kbar (Groppo et al., 2016).

4. **Methods**

188 Double polished wafers with a thickness of about 0.4 ± 0.2 mm were prepared from the samples
189 described in chapter 3. A microthermometric study was conducted on a Linkam THMSG 600
190 stage mounted on Olympus microscope at the Wadia Institute Fluid inclusion Laboratory. The
191 equations of Zhang and Frantz (1987) and Brown and Lamb (1989) were used for the estimation
192 of isochores of aqueous fluid inclusions, whereas the equation of Bower and Helgeson (1985)
193 was used for the calculation of isochores of CO_2 –H_2O inclusions in the "Flincor" computer
194 program of Brown (1989).
195
196 **5. Fluid inclusion petrography**
197 We have studied fluid inclusions hosted in garnet and in matrix quartz, as well as in quartz
198 included in garnet porphyroblasts belonging to the peak metamorphic mineral assemblage (i.e.
199 garnet + lawsonite + glaucophane + phengite + quartz ± omphacite; see Groppo et al., 2016).
200 Texturally, two types of fluid inclusions have been found: regular shaped inclusions (Type-I
201 and Type-II) and re-equilibrated inclusions (Type-III). Regular shaped inclusions are either
202 two-phase carbonic-aqueous (Type-I) or two-phase aqueous (Type-II) inclusions. Type-II
203 inclusions are more abundant than Type-I inclusions.
204 Type–I inclusions are two-phase inclusions (V_{CO2} + L_{H2O}) at room temperature (~ 27°C) and
205 contain an aqueous-carbonic fluid (Fig. 3A, B). The size of these inclusions are small (average
206 of 9 μm). The CO_2 vapour has a variable volume proportion ranging from 10 to 30% of the total
207 volume of the inclusion. These inclusions are systematically found as isolated occurrences
208 within garnet and quartz, and are dispersed randomly in the host grains (Fig. 3A, B), therefore
209 they have been interpreted as primary in origin; moreover, because garnet is a peak phase, Type-
210 I inclusions have been entrapped at peak P-T conditions.
211 Type-II inclusions are two-phase aqueous (V_{H2O} + L_{H2O}) inclusions and are further classified as
212 Type-IIa and Type-IIb on the basis of their mode of occurrence. The size of these types of

inclusion ranges between 9 and 15 μm. Type-IIa inclusions are isolated and randomly distributed in the matrix quartz as well as in quartz included in garnet grains, and are therefore interpreted as primary inclusions; they were likely entrapped at, or near to, peak P-T conditions because quartz included in garnet is a prograde-to-peak phase. Type-IIb are concentrated along microfractures of the host minerals and are interpreted as secondary inclusions. The trails of the secondary inclusions often cross-cut the grain margins (i.e. transgranular inclusions) (Fig. 3C, D).

Type-III inclusions are re-equilibrated inclusions showing partially dendridic type network as well as necking phenomena (Fig. 4A-D). The dendritic type network may be originated by the dissolution of inclusion walls, as well as by the closing of inclusion voids which lead to form numerous tails and channels filled by fluids (Invernizzi et al., 1998). Some inclusions show necking phenomena, and few also show "C" type microstructures. Some solitary inclusions surrounded by minute satellite inclusions are observed in matrix quartz.

6. Microthermometric results

Microthermometry reveals compositional variations of the fluid inclusions from aqueous-carbonic to aqueous. The results of microthermometric measurements are shown in histograms (Figs.5, 6 and 7) and summarized in Table 1.The Type-I aqueous-carbonic fluid inclusions hosted in the matrix quartz as well as in quartz included in garnet and in garnet itself, show initial melting temperature (Tim) between -56.9°C and -56.6°C, thus suggesting a nearly pure CO_2 composition for the vapour phase. The homogenization temperature of CO_2 in these inclusions lies between -7 to -2°C (Fig. 5B). The clathrate melting temperature was also observed in some carbonic-aqueous inclusions, which occurred between +7.1 to 8.6°C. The total homogenization of such inclusions took place in between 227° and 265°C (Fig. 5A).

The Type-II two-phase aqueous inclusions mainly occur in matrix quartz as well as in quartz included in garnet. Type-IIa primary inclusions and Type-IIb secondary inclusions show different initial melting temperature (Tim) and final melting temperature (Tfm) values. Type IIa primary H_2O-NaCl inclusions show Tim in the range −21.2°C to −22.6°C, Tfm of −5°C to −10°C (Fig. 6A) and temperature of homogenization (Th) between 250°C and 300°C (Fig. 7B). The corresponding salinity ranges are estimated at 7.8–13.98 wt% NaCl equivalent, with density of 0.863–0.874 g/cm^3. Type-IIb secondary two-phase aqueous inclusions occurring in transgranular trails show a wider range of Tim (−21° to −23 °C), and significantly different Tfm (−1° to -4°C; Fig. 6 B) and Th (145° to 220°C; Fig. 7A) values. The corresponding salinity ranges are estimated at 1.65–6.37 wt% NaCl equivalent, and density is in the range of 0.889–0.938 g/cm^3.

Composition and density of the fluid phase observed in the different generations of inclusions are used to calculate the isochores in the P–T space, and the implications are discussed in a later section. The minimum Th and the maximum Th obtained from the peak value in Figs. 5,6,7 for each inclusion type were considered for construction of isochores, following the criteria given by Touret (2001),.

7. Discussion

The study of fluid inclusions provides important constraints on their trapping conditions (textural evidence in relation to *P–T* estimates), composition and behaviour of metamorphic fluids. This is the first systematic fluid inclusion study on the blueschists from the Sapi-Shergol ophiolitic mélange that correlates P-T data from mineral geothermobarometry and fluid inclusions. Our results reveal the pervasive presence of aqueous-carbonic and aqueous fluids preserved in quartz and garnet.

7.1. Interpretation of fluid inclusions textures

In the studied samples, the isolated nature of Type-I aqueous-carbonic inclusions and of Type-IIa two-phase aqueous inclusions hosted in quartz and garnet reveals that they may have formed during the crystallization of their host minerals, and may thus be considered to be trapped early during the mineral growth (Roedder, 1984). Moreover, because garnet is a peak phase, the primary Type-I and Type-IIa inclusions have been entrapped at, or near to, peak P-T conditions. Type-IIb two-phase aqueous inclusions occur in transgranular trails and are therefore clearly secondary in nature.

Concerning Type-III inclusions, the most commonly observed features are: (i) necking, (ii) inclusions with 'C' or Arc shaped microstructure, (iii) satellite inclusions, (iv) hook shaped or annular inclusions, (v) dendritic network of inclusions (Fig.4 A, B, C & D). The necking textures are interpreted as related to intense dissolution of the inclusion walls to produce highly irregular inclusion morphology. These microtextures were likely formed along a decompression path: fractures initially developed along the inclusion planes in which inclusions primarily necked down, and later on they were stretched (Fig 4C). The inclusions displaying a hook-like morphology or annular textures (Fig.4C) are similar to inclusions formed under isothermal decompression (ITD), as shown in the experimental work of Sterner and Bodnar (1989), Vityk and Bodnar (1995), and Bodnar (2003). Boullier et al. (1991) proposed that annular textures are symptomatic of an anisotropic stress environment. Satellite inclusions around a bigger solitary inclusion are analogous to 'explosion' textures described for natural and synthetic fluid inclusions in quartz that have experienced overpressures caused by 'near isothermal decompression' (e.g., Bodnar et al., 1989; Vityk et al., 1994; Vityk and Bodnar,1995). Opposite to these microtextures which are related to decompression, the development of dendritic networks of imploded inclusions in quartz is indicative of near isobaric cooling (IBC) in the last stages of metamorphic evolution. This type of texture is similar to that described by Vityk

et al. (1994) and Vityk and Bodnar (1995) for their experimental work during isobaric cooling (IBC).

7.2. Nature and Source of Fluids

Two types of fluid (aqueous-carbonic and aqueous) have been found in the blueschist mineral assemblage. Type-I aqueous-carbonic fluids occur as primary inclusions in peak metamorphic garnet as well as in quartz. Type-IIa aqueous fluid with high saline nature is preserved as primary inclusions in matrix quartz, as well as in quartz included in garnet, whereas Type-IIb aqueous fluid with low saline nature is observed as secondary inclusions in quartz.

Type-I aqueous-carbonic inclusions have constant vapour: liquid ratios (i.e. 30:70). The temperature of clathrate melting and the homogenization temperature of the CO_2 phase in these inclusions indicate that they are predominantly aqueous with a small amount of CO_2, consistently with the stability of lawsonite at peak metamorphic conditions. According to Groppo et al. (2016), in fact, the contemporaneous growth of lawsonite and garnet would have been enhanced by a protracted H_2O influx at the relatively high pressure of ca. 17–18 kbar. The predominance of aqueous fluids in high P metamorphic assemblages is also shown in previous studies which call upon substantial fluid release at high P–T conditions (e.g. Clarke et al., 2006; Tsujimori and Ernst, 2014; Ulmer and Trommsdorff, 1995; Scambelluri et al., 2004; Poli and Schmidt, 1995; Poli et al., 2009) through metamorphic devolatilization reactions occurring in the subducting slab (Bebout, 1991, 1995; Jarrard, 2003).

7.3. Reconstruction of the P-T-fluid history

P–T estimates based on conventional thermobarometry proposed peak conditions of 350–420 °C, 9–11 kbar for the Sapi-Shergol blueschists (Honegger et al., 1989). Petrologic modeling performed by our research team (Groppo et al., 2016) inferred peak P–T conditions significantly

312 higher than those previously estimated, i.e. ca. 470 °C, 19 kbar. According to Groppo et al.
313 (2016), the estimated peak metamorphic conditions suggest that the blueschists experienced a
314 cold subduction history along a very low to low thermal gradient ("early" prograde: ca. 5–6
315 °C/km; "late" prograde: ca. 7–8 °C/km). The preservation of lawsonite in the studied lithologies
316 further indicate that the exhumation process must have been coupled with substantial cooling
317 (i.e. without crossing the lawsonite-out boundary; Zack et al., 2004).
318 As concerning the fluid evolution, isochores are plotted in comparison with the *P–T* path
319 inferred on the basis of thermodynamic modelling and thermobarometry (Fig. 8). Isochores of
320 both Type-I aqueous–carbonic inclusions and Type-II aqueous inclusions plot in the lower part
321 of the P–T space. Although these inclusions are texturally primary and are hosted within peak
322 minerals (garnet and quartz included in garnet), they do not plot along the prograde *P–T* path
323 or at peak metamorphic conditions, thus suggesting that these inclusions must have experienced
324 considerable leakage and re-equilibration, resulting in only low-density fluid eventually
325 preserved in the inclusions. Therefore, it is assumed that Type-I CO_2-H_2O and Type-IIa aqueous
326 inclusions most likely formed at or near the peak *P–T* conditions at ~ 19 kbar, ~ 450°C, but
327 they were later re-equilibrated during exhumation. The isochores of secondary aqueous
328 inclusions (Type IIa) plots above the isochores of primary inclusions because the secondary
329 aqueous inclusions originate at lower temperature and their densities are thus higher (Fig.8).
330 Evidences of such a pervasive re-equilibration are very clearly represented by the textural
331 features of Type-III fluid inclusions described in the previous chapters (Fig.4). The observed
332 textural features are indicative either of re-equilibration occurred during isothermal
333 decompression, as well as during isobaric cooling at the final stages of exhumation. Similar
334 high degrees of re-equilibration of fluid inclusions during retrogression is well documented by
335 Sterner and Bodnar (1989) and Kuster and Stockhert (1997) for high-P and low-T rocks. We
336 therefore suggest that these re-equilibrated inclusions might have been trapped during the early

337 stages of subduction, while their re-equilibration took place during the subsequent fast
338 exhumation. Such high internal underpressure at low temperature would develop only when the
339 subduction / burial path is very steep and consequently follows very low geothermal gradients;
340 the preservation of lawsonite in the studied blueschist facies lithologies strongly support the
341 scenario in which very low geothermal gradients were prevailing during initial subduction as
342 well as during exhumation (Fig. 8). The presence of dendritic network type inclusions suggests
343 isobaric cooling (as evidenced by the experimental studies of Bodnar et al., 1989; Vityk et al.,
344 1994; Vityk and Bodnar, 1995). The hook like inclusions were likely trapped at about 3 kbar
345 (Vityk and Bodnar, 1995), whereas the implosion texture formed at higher pressure (Boulier,
346 1999). In our case, the last stage of the P-T evolution is represented by the isobaric cooling after
347 the isothermal decompression, therefore we suggest that the dendritic morphology might have
348 been formed at this last stage (Fig. 8). This interpretation is clearly compatible with the broad
349 geological setting of the area.
350

351 **8. Conclusions**

352 The first detailed fluid inclusions study of Himalayan blueschist-facies lithologies from the
353 Sapi-Shergol ophiolitic mélange in the Indus suture zone, revealed predominantly CO_2–H_2O
354 and H_2O-NaCl inclusions. The primary CO_2-H_2O and H_2O-NaCl inclusions were trapped by
355 host minerals at peak P-T conditions. The fluid was most likely produced through metamorphic
356 devolatilization reactions occurring in the subducting slab. Additional multiple generations of
357 re-equilibrated inclusions show characteristic morphologies developed in response to fast rates
358 of uplift. A nearly isothermal decompression path followed peak metamorphic P-T condition
359 and is characterized by stretching, necking and formation of "C" or hook-like shaped inclusions.
360 A veining stage is associated to late isobaric cooling and is characterized by the local
361 development of a dendritic network of fluid inclusions.

Acknowledgments

HKS, AK, PCS and ST are thankful to the Director of the Wadia Institute of Himalayan Geology, Dehradun, for providing lab facilities and encouragement to carry out this work. An nonymous reviewer and the journal editor provided useful suggestions, which led to significant improvement of the manuscript. This study is part of a Cooperation Agreement between the Wadia Institute of Himalayan Geology (Dehradun, India) and the University of Torino, Dept. of Earth Sciences (Torino, Italy). Fieldwork of FR and CG was supported by University of Torino—Call 1—Junior PI Grant (TO_Call1_2012_0068).

References

Abers, G. A., Nakajima, J., van Keken, P. E., Kita, S., Hacker, B. R., 2013. Thermal–petrological controls on the location of earthquakes within subducting plates. Earth and Planetary Science Letters 369, 178-187.

Ahmad, T., Islam, R., Khanna, P. P., Thakur, V. C., 1996. Geochemistry, petrogenesis and tectonic significance of the basic volcanic units of the Zildat ophiolitic mélange, Indus suture zone, eastern Ladakh (India). Geodinamica Acta 9, 222-233.

Ao, A., Bhowmik, S. K., 2014. Cold subduction of the Neotethys: the metamorphic record from finely banded lawsonite and epidote blueschists and associated metabasalts of the Nagaland Ophiolite Complex, India. Journal of Metamorphic Geology 32, 829-860.

Bakker, R. J., Mamtani, M. A., 2000. Fluid inclusions as metamorphic process indicators in the Southern Aravalli Mountain Belt (India). Contributions to Mineralogy and Petrology 139, 163-179.

Barker, A. J., 1995. Post-entrapment modification of fluid inclusions due to overpressure: evidence from natural samples. Journal of Metamorphic Geology 13, 737-750.

Barr, H., 1990. Preliminary fluid inclusion studies in a high-grade blueschist terrain, Syros, Greece. Mineralogical Magazine 54, 159-168.

Bebout, G. E., 1991. Field-based evidence for devolatilization in subduction zones: Implications for are magmatism. Science 251, 413-416.

Bebout, G. E., 1995. The impact of subduction-zone metamorphism on mantle-ocean chemical cycling. Chemical Geology 126, 191-218.

Bodnar, R. J., 2003. Reequilibration of fluid inclusions. Fluid inclusions: Analysis and interpretation 32, 213-230.

394 Bodnar, R. J., Binns, P. R., Hall, D. L., 1989. Synthetic fluid inclusions-VI. Quantitative
395 evaluation of the decrepitation behaviour of fluid inclusions in quartz at one atmosphere
396 confining pressure. Journal of Metamorphic Geology 7, 229-242.
397 Boullier, A. M., France-Lanord, C., Dubessy, J., Adamy, J., Champenois, M., 1991. Linked
398 fluid and tectonic evolution in the High Himalaya mountains (Nepal). Contributions to
399 Mineralogy and Petrology 107, 358-372.
400 Bowers, T. S., Helgeson, H. C., 1983. Calculation of the thermodynamic and geochemical
401 consequences of nonideal mixing in the system H_2O-CO_2-NaCl on phase relations in geologic
402 systems: Equation of state for H_2O-CO_2-NaCl fluids at high pressures and temperatures.
403 Geochimica et Cosmochimica Acta 47, 1247-1275.
404 Brovarone, A. V., Groppo, C., Hetényi, G., Compagnoni, R., Malavieille, J., 2011. Coexistence
405 of lawsonite-bearing eclogite and blueschist: phase equilibria modelling of Alpine Corsica
406 metabasalts and petrological evolution of subducting slabs. Journal of Metamorphic Geology
407 29, 583-600.
408 Brown, P. E., 1989. FLINCOR; a microcomputer program for the reduction and investigation
409 of fluid-inclusion data. American Mineralogist 74, 1390-1393.
410 Brown, P. E., Lamb, W. M., 1989. P-V-T properties of fluids in the system H_2O±CO_2±NaCl:
411 New graphical presentations and implications for fluid inclusion studies. Geochimica et
412 Cosmochimica Acta 53, 1209-1221.
413 Cao, Y., Jung, H., Song, S., 2013. Petro-fabrics and seismic properties of blueschist and eclogite
414 in the North Qilian suture zone, NW China: Implications for the low-velocity upper layer in
415 subducting slab, trench-parallel seismic anisotropy, and eclogite detectability in the subduction
416 zone. Journal of Geophysical Research: Solid Earth 118, 3037-3058.

417 Chantel, J., Mookherjee, M., Frost, D. J., 2012. The elasticity of lawsonite at high pressure and
418 the origin of low velocity layers in subduction zones. Earth and Planetary Science Letters 349,
419 116-125.
420 Chatterjee, N., Ghose, N. C., 2010. Metamorphic evolution of the Naga Hills eclogite and
421 blueschist, Northeast India: implications for early subduction of the Indian plate under the
422 Burma microplate. Journal of Metamorphic Geology 28, 209-225.
423 Clarke, G. L., Powell, R., Fitzherbert, J. A., 2006. The lawsonite paradox: a comparison of field
424 evidence and mineral equilibria modelling. Journal of Metamorphic Geology 24, 715-725.
425 El-Shazly, A. K., Sisson, V. B., 1999. Retrograde evolution of eclogite facies rocks from NE
426 Oman: evidence from fluid inclusions and petrological data. Chemical Geology 154, 193-223.
427 Ferrando, S., Rolfo, F., Lombardo, B., 2007. Fluid evolution from metamorphic peak to
428 exhumation in Himalayan granulitised eclogites, Ama Drime range, southern Tibet. Eur. J.
429 Mineral. 19, 439–461.
430 Frank, W., Gansser, A., Trommsdorff, V., 1977. Geological observations in the Ladakh area
431 (Himalayas): a preliminary report. Schweiz. mineral. petrogr. Mitt 57, 89-113.
432 Gao, J., Klemd, R., 2001. Primary fluids entrapped at blueschist to eclogite transition: evidence
433 from the Tianshan meta-subduction complex in northwestern China. Contributions to
434 Mineralogy and Petrology 142, 1-14.
435 Ghose, N. C., Singh, M. R., 1980. Occurrence of blueschist facies in the ophiolite belt of Naga
436 Hills, east of Kiphire, NE India. Geologische Rundschau 69, 41-48.
437 Giaramita, M. J., Sorensen, S. S., 1994. Primary fluids in low-temperature eclogites: evidence
438 from two subduction complexes (Dominican Republic, and California, USA). Contributions to
439 Mineralogy and Petrology 117, 279-292.

440 Groppo, C., Rolfo, F., Sachan, H. K., Rai, S. K., 2016. Petrology of blueschist from the Western
441 Himalaya (Ladakh, NW India): Exploring the complex behavior of a lawsonite-bearing system
442 in a paleo-accretionary setting. Lithos 252, 41-56.
443 Guillot, S., Mahéo, G., de Sigoyer, J., Hattori, K.H. Pecher, A., 2008. Tethyan and Indian
444 subduction viewed from the Himalayan high- to ultrahigh-pressure metamorphic rocks.
445 Tectonophysics 451, 225–241.
446 Hames, W. E., Tracy, R. J., Bodnar, R. J., 1989. Postmetamorphic unroofing history deduced
447 from petrology, fluid inclusions, thermochronometry, and thermal modeling: An example from
448 southwestern New England. Geology 17, 727-730.
449 Hollister, L. S., Burruss, R. C., Henry, D. L., Hendel, E. M., 1979. Physical conditions during
450 uplift of metamorphic terranes, as recorded by fluid inclusions. Bulletin de Mineralogie 102,
451 555-561.
452 Honegger, K., Le Fort, P., Mascle, G., Zimmermann, J. L., 1989. The blueschists along the
453 Indus suture zone in Ladakh, NW Himalaya. Journal of Metamorphic Geology 7, 57-72.
454 Invernizzi, C., Vityk, M., Cello, G., Bodnar, R., 1998. Fluid inclusions in high pressure/low
455 temperature rocks from the Calabrian Arc (Southern Italy): the burial and exhumation history
456 of the subduction-related Diamante-Terranova unit. Journal of Metamorphic Geology 16, 247-
457 258.
458 Jarrard, R. D., 2003. Subduction fluxes of water, carbon dioxide, chlorine, and potassium.
459 Geochemistry, Geophysics, Geosystems, 4(5).
460 Kim, D., Katayama, I., Michibayashi, K., Tsujimori, T., 2013. Deformation fabrics of natural
461 blueschists and implications for seismic anisotropy in subducting oceanic crust. Physics of the
462 Earth and Planetary Interiors 222, 8-21.

463 Klemd, R., 1989. PT evolution and fluid inclusion characteristics of retrograded eclogites,
464 Münchberg Gneiss Complex, Germany. Contributions to Mineralogy and Petrology 102, 221-
465 229.
466 Klemd, R., Van den Kerkhof, A. M., Horn, E. E., 1992. High-density $CO_2 - N_2$ inclusions in
467 eclogite-facies metasediments of the Münchberg gneiss complex, SE Germany. Contributions
468 to Mineralogy and Petrology 111, 409-419.
469 Küster, M., Stöckhert, B., 1997. Density changes of fluid inclusions in high-pressure low-
470 temperature metamorphic rocks from Crete: a thermobarometric approach based on the creep
471 strength of the host minerals. Lithos 41, 151-167.
472 Lombardo, B. Rolfo, F., 2000. Two contrasting eclogite types in the Himalayas: implications
473 for the Himalayan orogeny. Journal of Geodynamics 30, 37–60.
474 Luckscheiter, B., Morteani, G., 1980. Microthermometrical and chemical studies of fluid
475 inclusions in minerals from Alpine veins from the penninic rocks of the central and western
476 Tauern Window (Austria/Italy). Lithos 13, 61-77.
477 Mahéo, G., Fayoux, C., Guillot, S., Garzanti, E., Capiez, P., Mascle, G., 2006. Geochemistry
478 of ophiolitic rocks and blueschists from the Sapi-Shergol mélange (Ladakh, NW Himalaya,
479 India): implication for the timing of the closure of the Neo-Tethys ocean. Journal of Asian Earth
480 Sciences 26, 695-707.
481 Martin, L. A., Wood, B. J., Turner, S., Rushmer, T., 2011. Experimental measurements of trace
482 element partitioning between lawsonite, zoisite and fluid and their implication for the
483 composition of arc magmas. Journal of Petrology, egr018.
484 Mukherjee, B. K., Sachan, H. K., 2009. Behavior of fluids in coesite bearing rocks of Tso-
485 Morari region, NW Himalaya: Implication for exhumation process. Geological Magazine 146,
486 876-889.

Poli, S., Schmidt, M. W., 1995. H_2O transport and release in subduction zones: experimental constraints on basaltic and andesitic systems. Journal of Geophysical Research: Solid Earth 100(B11), 22299-22314.

Poli, S., Franzolin, E., Fumagalli, P., Crottini, A., 2009. The transport of carbon and hydrogen in subducted oceanic crust: an experimental study to 5 GPa. Earth and Planetary Science Letters 278, 350-360.

Reuber, I., Colchen, M., Mevel, C., 1987. The geodynamic evolution of the South-Tethyan, margin in Zanskar, NW-Himalaya, as revealed by the Spongtang ophiolitic mélanges. Geodinamica Acta 1, 283-296.

Robertson, A. H. F., 2000. Formation of mélanges in the Indus suture zone, Ladakh Himalaya by successive subduction-related, collisional and post-collisional processes during late Mesozoic-late Tertiary time. Geological Society, London, Special Publications 170, 333-374.

Roedder, E., 1984. Fluid Inclusions (Reviews in Mineralogy, Vol. 12) Mineralogical Society of America. Washington, DC.

Rolfo, F., Lombardo, B., Compagnoni, R., Le Fort, P., Lemennicier, Y., Pêcher, A., 1997. Geology and Metamorphism of the Ladakh Terrane and Shyok Suture Zone in the Chogo Lungma - Turmik area (northern Pakistan). Geodinamica Acta 10, 251-270.

Sachan, H. K., Mukherjee, B. K., 2001. Evidences of fluid re-equilibration in blueschist rocks from Shergol Ophiolitic Mélange, Indus Suture Zone, Ladakh. Himalayan Geology 22, 127-133.

Santosh, M., 1987. Cordierite gneisses of southern Kerala, India: petrology, fluid inclusions and implications for crustal uplift history. Contributions to Mineralogy and Petrology 96, 343-356.

Scambelluri, M., 1992. Retrograde fluid inclusions in eclogitic metagabbros from the Ligurian Western Alps. European journal of mineralogy 4, 1097-1112.

512 Scambelluri, M., Philippot, P., 2001. Deep fluids in subduction zones. Lithos 55, 213-227.
513 Scambelluri, M., Müntener, O., Ottolini, L., Pettke, T. T., Vannucci, R., 2004. The fate of B,
514 Cl and Li in the subducted oceanic mantle and in the antigorite breakdown fluids. Earth and
515 Planetary Science Letters 222, 217-234.
516 Selverstone, J., Spear, F.S., 1985. Metamorphic P–T Paths from pelitic schists and greenstones
517 from the south-west Tauern Window, Eastern Alps. Journal of metamorphic Geology 3, 439-
518 465.
519 Shams, F. A., 1972. Glaucophane-bearing rocks from near Topsin, Swat. First record from
520 Pakistan. Pakistan Journal of Scientific Research 24, 343-345.
521 Sisson, V. B., Hollister, L. S., Onstott, T. C., 1989. Petrologic and age constraints on the origin
522 of a low-pressure/high-temperature metamorphic complex, southern Alaska. Journal of
523 Geophysical Research: Solid Earth 94(B4), 4392-4410.
524 Spandler, C., Pirard, C., 2013. Element recycling from subducting slabs to arc crust: A review.
525 Lithos 170, 208-223.
526 Sterner, S. M., Bodnar, R. J., 1989. Synthetic fluid inclusions-VII. Re-equilibration of fluid
527 inclusions in quartz during laboratory-simulated metamorphic burial and uplift. Journal of
528 Metamorphic Geology 7, 243-260.
529 Sterner, S. M., Hall, D. L., Keppler, H., 1995. Compositional re-equilibration of fluid inclusions
530 in quartz. Contributions to Mineralogy and Petrology 119, 1-15.
531 Thakur, V., Misra, D., 1984. Tectonic framework of the Indus and Shyok suture zones in eastern
532 Ladakh, northwest Himalaya. Tectonophysics 101, 207-220.
533 Touret, J. L., 2001. Fluids in metamorphic rocks. Lithos 55, 1-25.
534 Touret, J., Van Hinte, J. E., 1992. Le rôle des fluides dans les zones de subduction: un séminaire
535 du Collège de France aux Pays-Bas. Proceedings of the Koninklijke Nederlandse Akademie
536 van Wetenschappen 95, 293-296.

537 Tsujimori, T., Ernst, W. G., 2014. Lawsonite blueschists and lawsonite eclogites as proxies for
538 palaeo-subduction zone processes: a review. Journal of Metamorphic Geology 32, 437-454.
539 Ulmer, P., Trommsdorff, V., 1995. Serpentine stability to mantle depths and subduction-related
540 magmatism. Science 268(5212), 858.
541 Vallis, F., Scambelluri, M., 1996. Redistribution of high-pressure fluids during retrograde
542 metamorphism of eclogite-facies rocks (Voltri Massif, Italian Western Alps). Lithos 39, 81-92.
543 Van den Kerkhof, A. M., Hein, U. F., 2001. Fluid inclusion petrography. Lithos 55, 27-47.
544 Virdi, N. S., Thakur, V. C., Kumar, S., 1977. Blueschist facies metamorphism from the Indus
545 suture zone of Ladakh and its significance. Himalayan Geology 7, 479-482.
546 Vityk, M. O., Bodnar, R. J., 1995. Textural evolution of synthetic fluid inclusions in quartz
547 during reequilibration, with applications to tectonic reconstruction. Contributions to
548 Mineralogy and Petrology 121, 309-323.
549 Vityk, M. O., Bodnar, R. J., Schmidt, C. S., 1994. Fluid inclusions as tectonothermobarometers:
550 Relation between pressure-temperature history and reequilibration morphology during crustal
551 thickening. Geology 22, 731-734.
552 Vry, J. K., Brown, P. E., 1991. Texturally-early fluid inclusions in garnets: evidence of the
553 prograde metamorphic path? Contributions to Mineralogy and Petrology 108, 271-282.
554 Winslow, D. M., Bodnar, R. J., Tracy, R. J., 1994. Fluid inclusion evidence for an anticlockwise
555 metamorphic P-T path in central Massachusetts. Journal of Metamorphic Geology 12, 361-371.
556 Xiao, Y., Hoefs, J., van den Kerkhof, A. M., Fiebig, J., Zheng, Y., 2000. Fluid history of UHP
557 metamorphism in Dabie Shan, China: a fluid inclusion and oxygen isotope study on the coesite-
558 bearing eclogite from Bixiling. Contributions to Mineralogy and Petrology 139, 1-16.
559 Zack, T., Rivers, T., Brumm, R., Kronz, A., 2004. Cold subduction of oceanic crust:
560 implications from a lawsonite eclogite from the Dominican Republic. European Journal of
561 Mineralogy 16, 909-916.

562 Zhang, Y. G., Frantz, J. D., 1987. Determination of the homogenization temperatures and
563 densities of supercritical fluids in the system NaCl-KCl-$CaCl_2$-H_2O using synthetic fluid
564 inclusions. Chemical Geology 64, 335-350.

565 **Figure Captions**

566 **Figure 1.** (A) Regional Geological Map of Ladakh Himalaya (adopted from Thakur and
567 Misra, 1984, and Mahéo et al., 2006); (B) Geological map of Shergol ophiolitic mélange
568 (after Honegger et al., 1989).

569

570 **Figure 2.** Representative microstructures of the studied blueschists. **Sample 14-4B: (a)**
571 Glaucophane + phengite + lawsonite layers alternated to discontinuous quartz-rich layers. Plane
572 Polarized Light (PPL); **(b)** Glaucophane + phengite + lawsonite layer containing variably sized
573 garnet Crosse Polarized Light (XPL); **(c)** Fine-grained idioblasts of lawsonite occur in
574 association with glaucophane (PPL); **Sample 14-6F/G: (d, e)** Glaucophane with minor
575 phengite defines the main foliation. The foliation is overgrown by lawsonite and garnet
576 porphyroblasts (PPL); **(f)** Lawsonite porphyroblast is crosscut by thin quartz veins (XPL).

577

578 **Figure 3.** Representative photomicrographs of Type-I and Type-II fluid inclusions (PPL). **(a)**
579 Type-I primary two-phase carbonic-aqueous inclusions in garnet (sample14-6F/G). **(b)** Type-I
580 primary two-phase aqueous-carbonic inclusions in matrix quartz (sample 14-4B). **(c)** Type-IIa
581 primary two-phase aqueous inclusions in quartz included in garnet (sample14-6F/G). **(d)** Type-
582 IIb secondary two-phase aqueous inclusions and Type-III re-equilibrated inclusions in quartz
583 (sample 14-4B).

584

585 **Figure 4.** Representative photomicrographs of Type-III fluid inclusions (PPL). **(a)** Re-
586 equilibrated inclusions in quartz showing implosion textures (sample14-6F/G). **(b)** Re-
587 equilibrated inclusions in quartz exhibiting necking and dendritic type networks of fluid
588 inclusions (sample14-6F/G). **(c)** Re-equilibrated inclusion in quartz showing different
589 morphologies: (i) hook-shape microstructure; (ii) “C” or “arc” shape, and (iii) necking and

590 stretched phenomena (sample 14-4B). **(d)** Dendritic type network of secondary fluid inclusions
591 in quartz (sample 14-4B).
592
593 **Figure 5.** Histograms showing **(a)** homogenization temperature (Th), and **(b)** final melting
594 temperature of CO_2 for Type-I CO_2-H_2O primary inclusions hosted in quartz and garnet.
595
596 **Figure 6.** Histograms showing final melting temperature of **(a)** Type-IIa primary H_2O-NaCl
597 inclusions in quartz, and **(b)** Type-IIb secondary H_2O-NaCl inclusions in quartz.
598
599 **Figure 7.** Histograms showing homogenization temperature (Th) for **(a)** Type-IIa primary H_2O-
600 NaCl inclusions in quartz, and **(b)** Type-IIb secondary H_2O-NaCl inclusions in quartz.
601
602 **Figure 8.** Comparison between fluid inclusion isochores and the *P–T* path (thick arrow in pink)
603 recorded by blueschist from the Sapi-Shergol ophiolitic mélange (after Groppo et al., 2016).
604 The lawsonite boundary is drawn after Zack et al. (2004). The yellow box shows peak
605 metamorphic conditions. The retrograde path is mainly characterized by nearly isothermal
606 decompression (as evident from hook shaped, annular inclusions and explosion type textures).
607 The last portion of the P-T path is characterized by isobaric cooling (as constrained by the
608 development of dendritic type networks of inclusions).
609

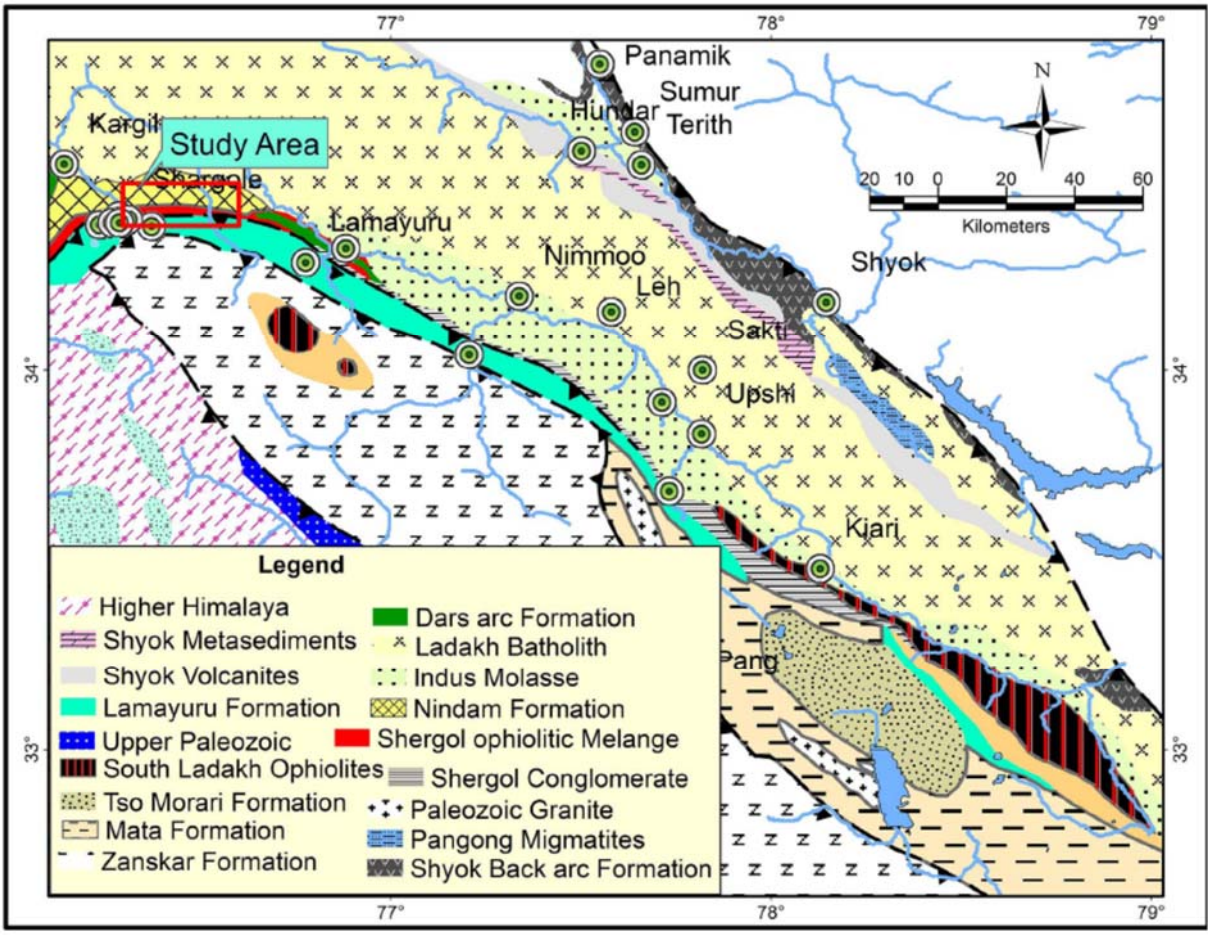

Fig. 1a

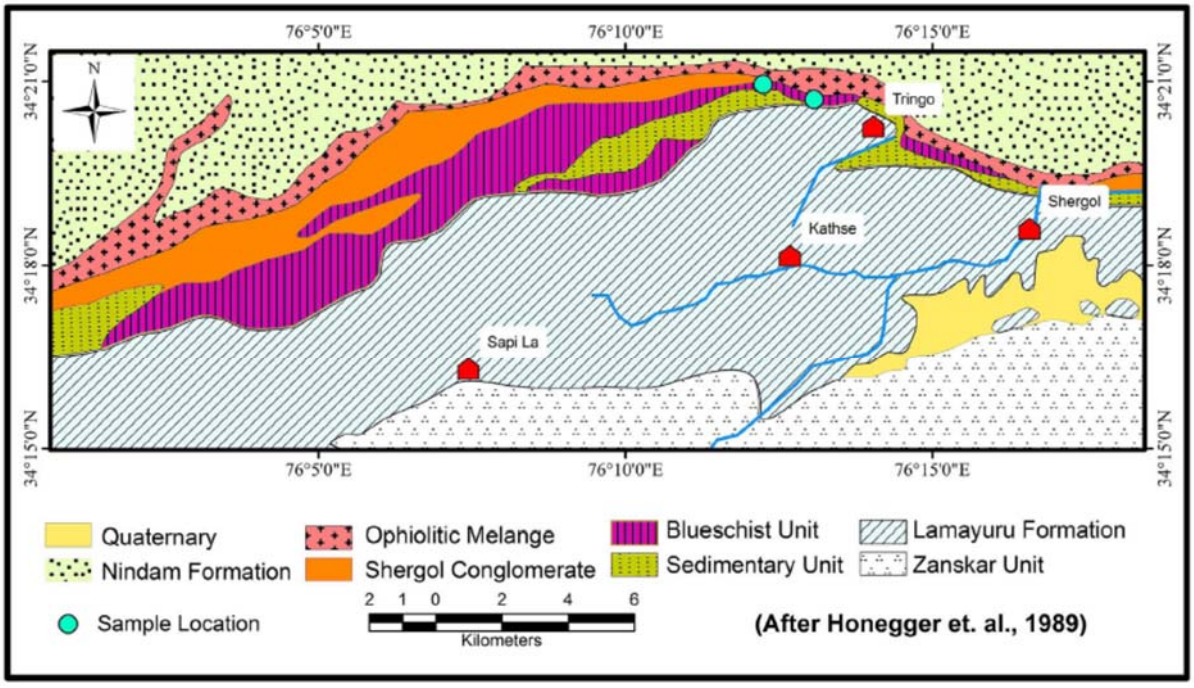

610

611 Fig. 1

612

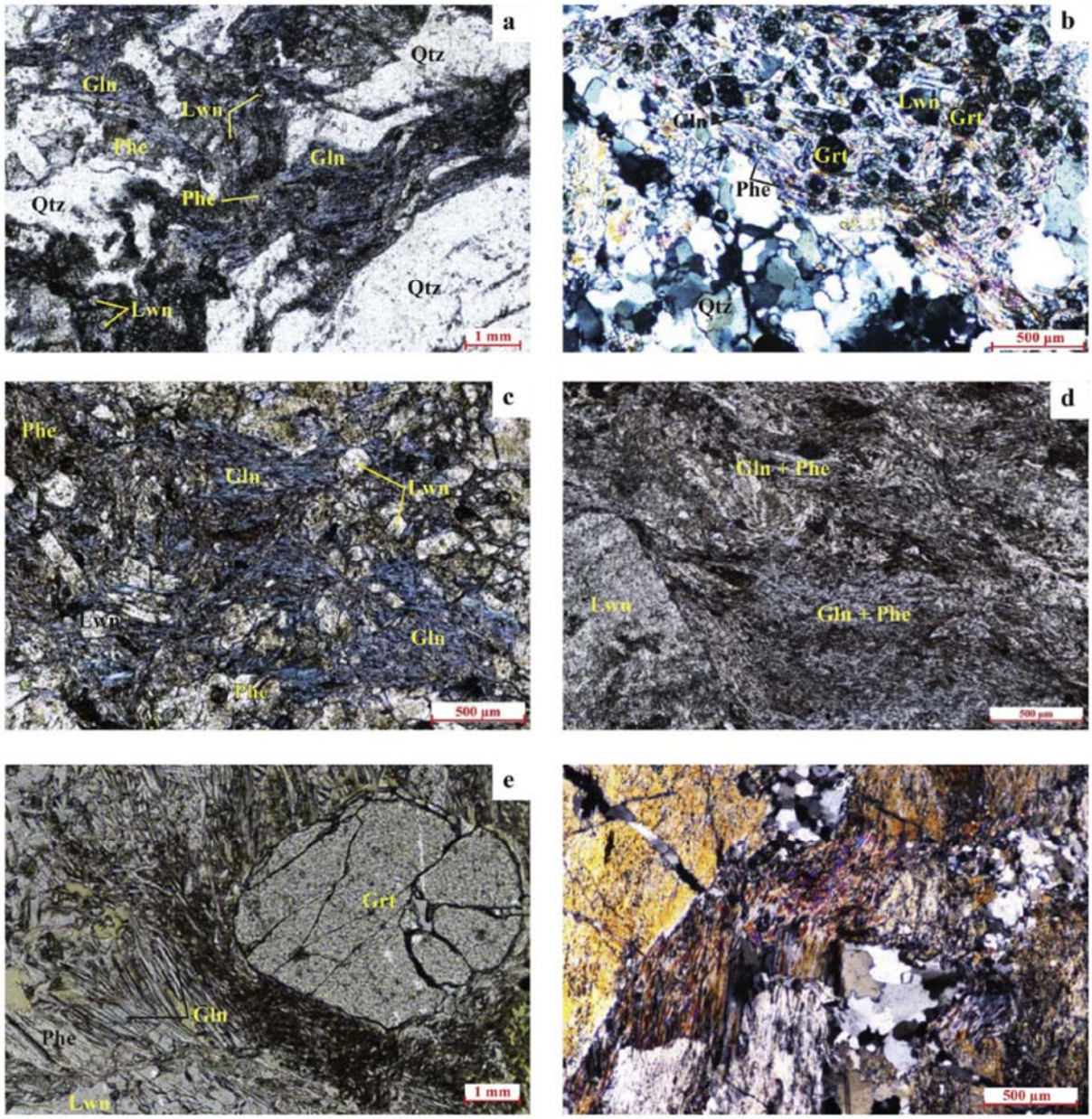
a
Qtz
Gln
Lwn
Phe
Gln
Phe
Qtz
Qtz
Lwn
1 mm
b
Gln
Lwn
Grt
Grt
Phe
Qtz
500 µm
c
Phe
Gln
Lwn
Lwn
Gln
Phe
500 µm
d
Gln + Phe
Lwn
Gln + Phe
500 µm
e
Grt
Gln
Phe
Lwn
1 mm
500 µm

Fig. 2

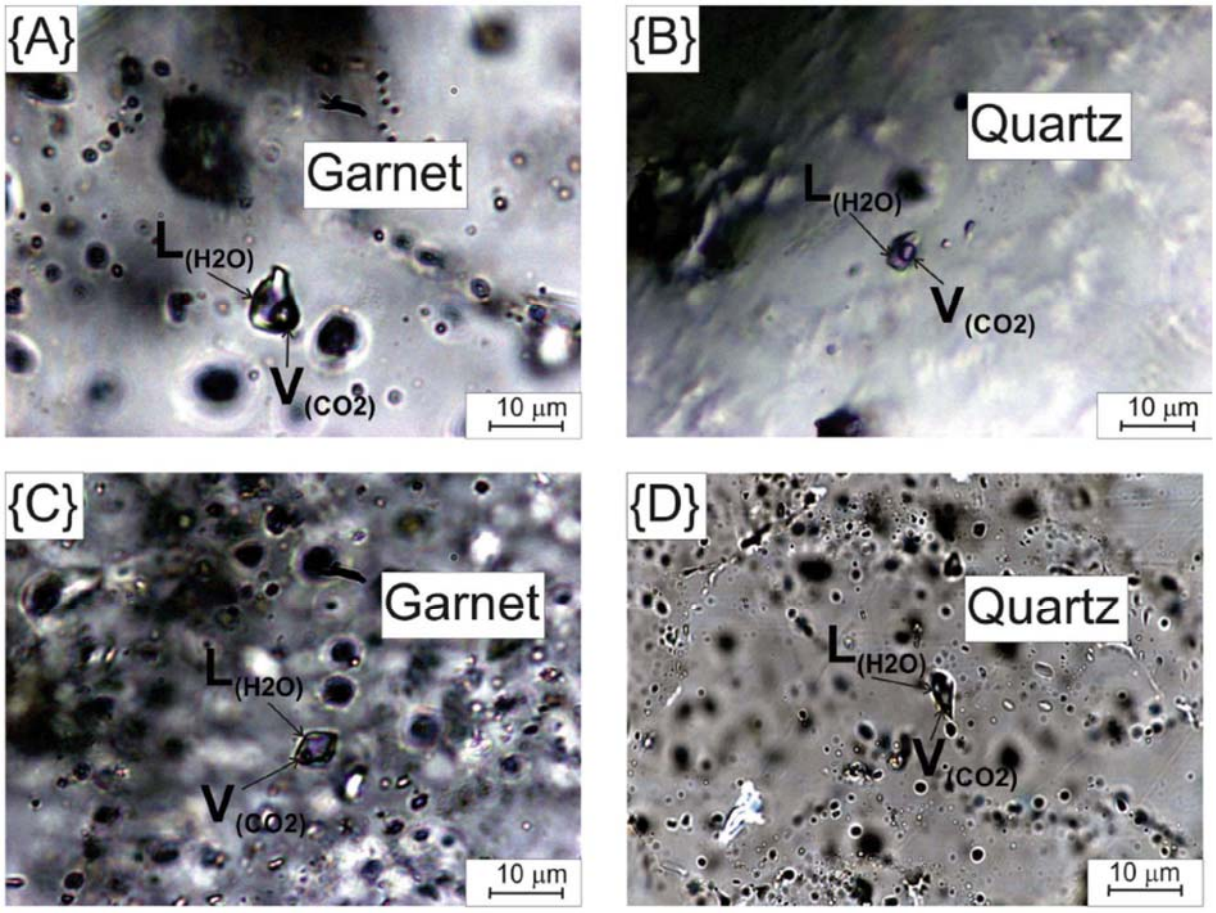
{A}
Garnet
L(H2O)
V(CO2)
10 µm
{B}
Quartz
L(H2O)
V(CO2)
10 µm
{C}
Garnet
L(H2O)
V(CO2)
10 µm
{D}
Quartz
L(H2O)
V(CO2)
10 µm

Fig. 3

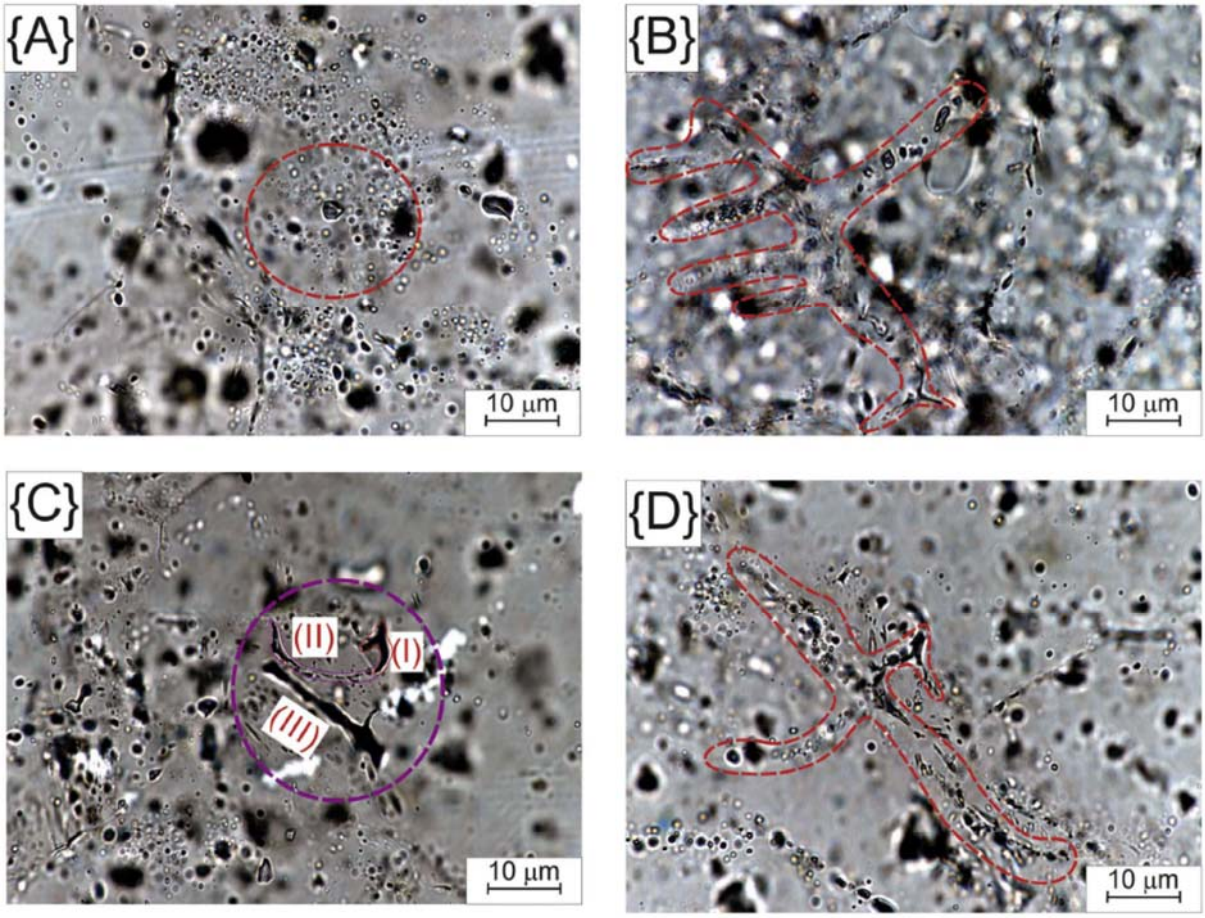

Fig. 4

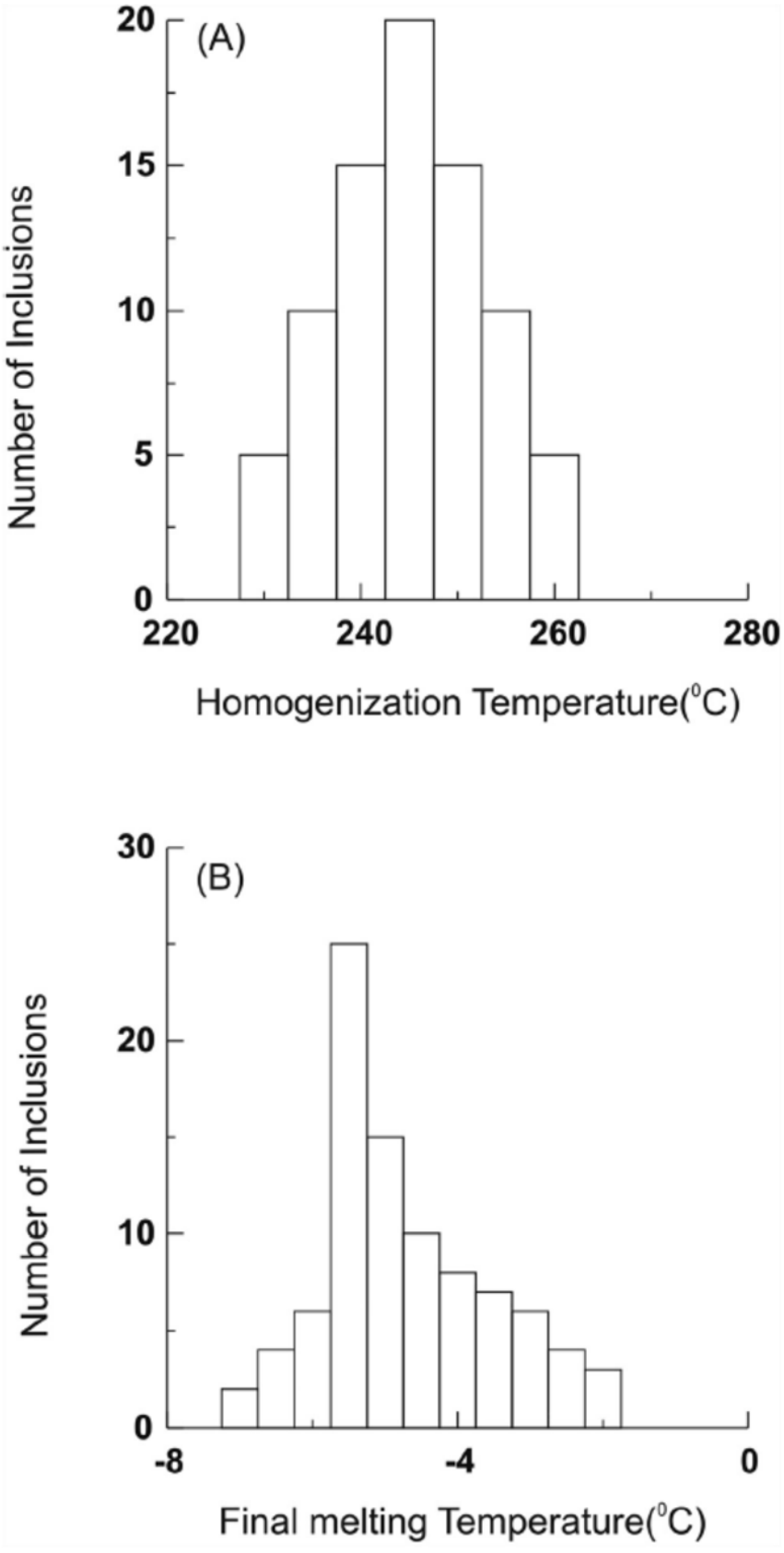

622

623 Fig. 5

624

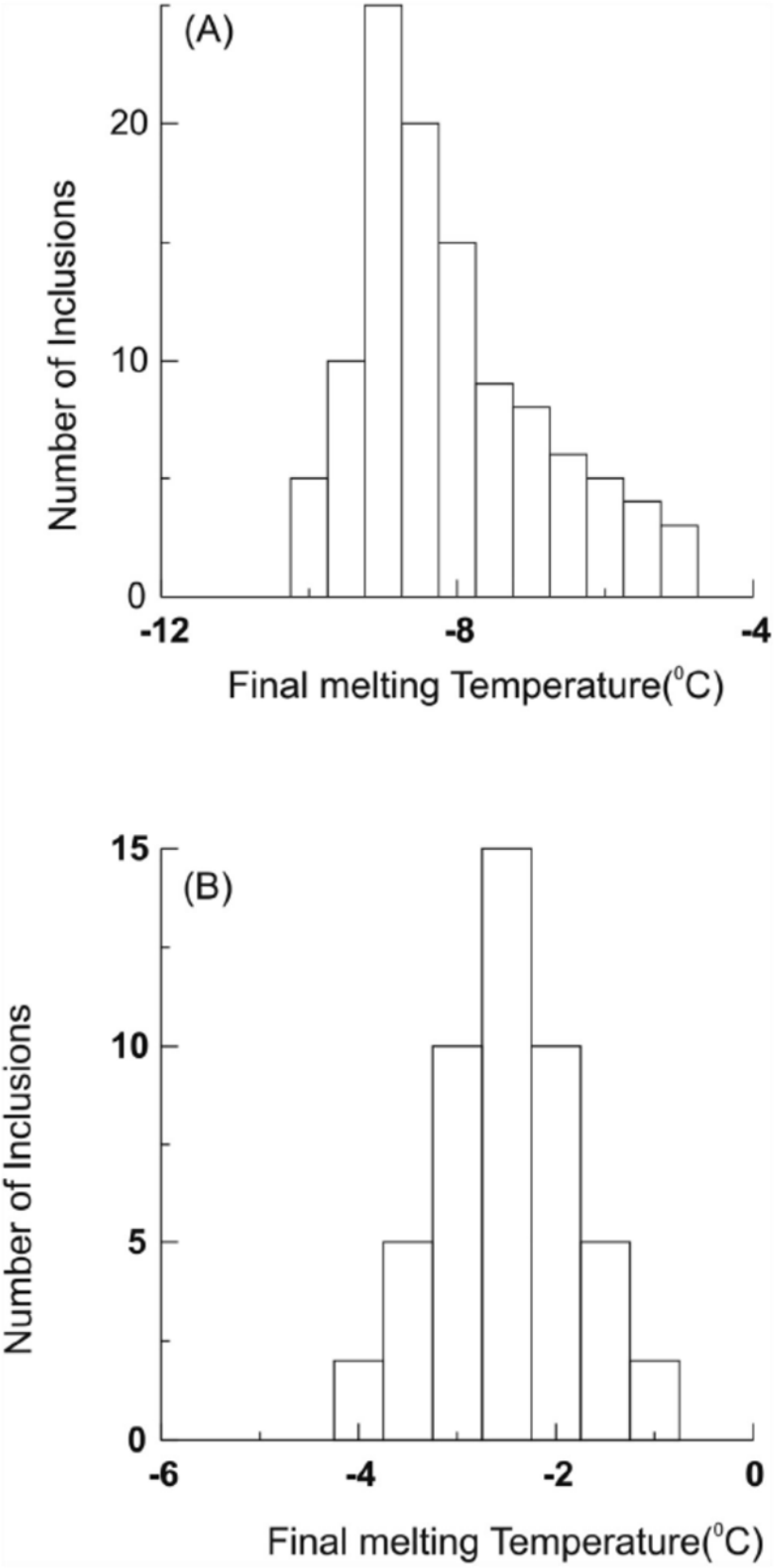

625

626 Fig. 6

627

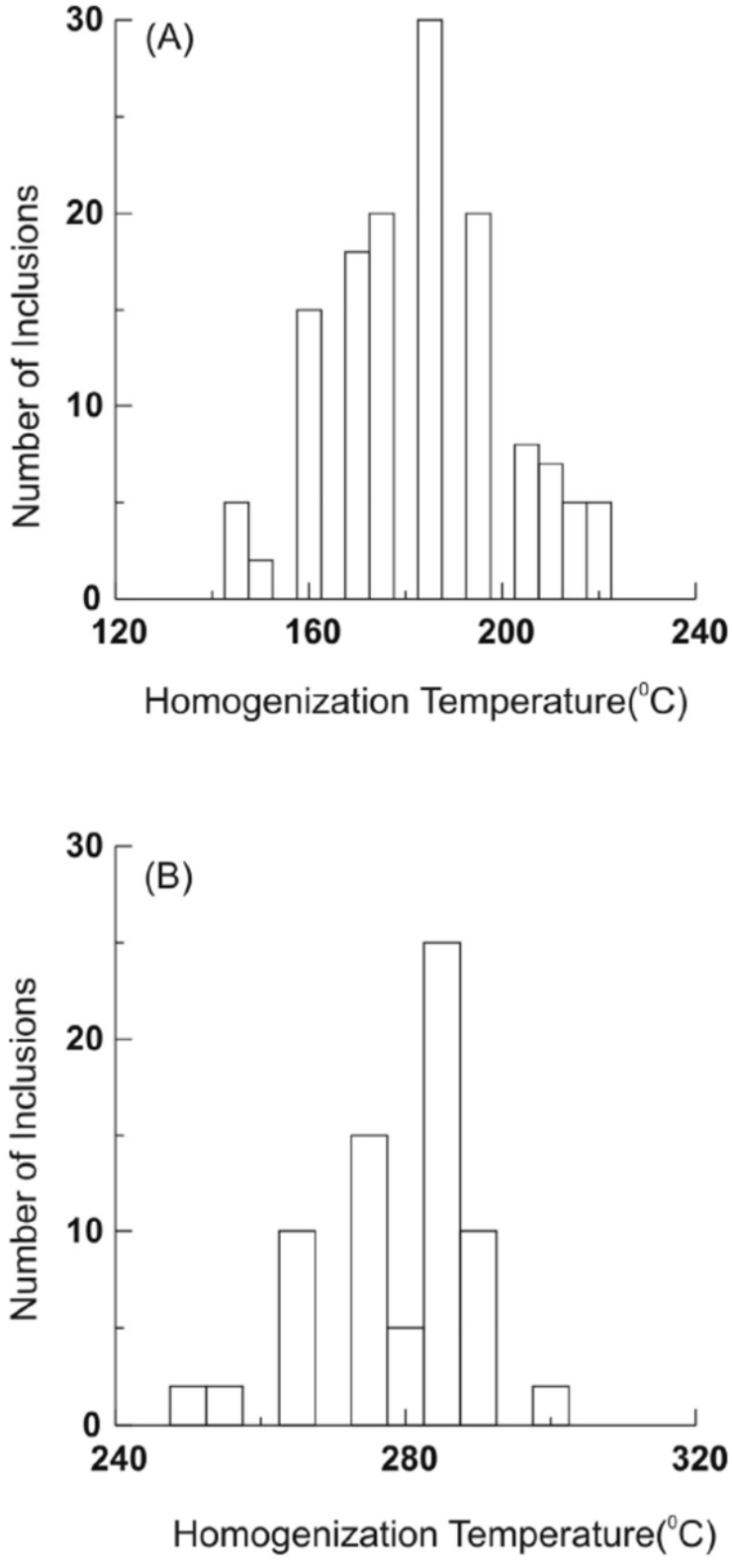

628

629 Fig- 7

630

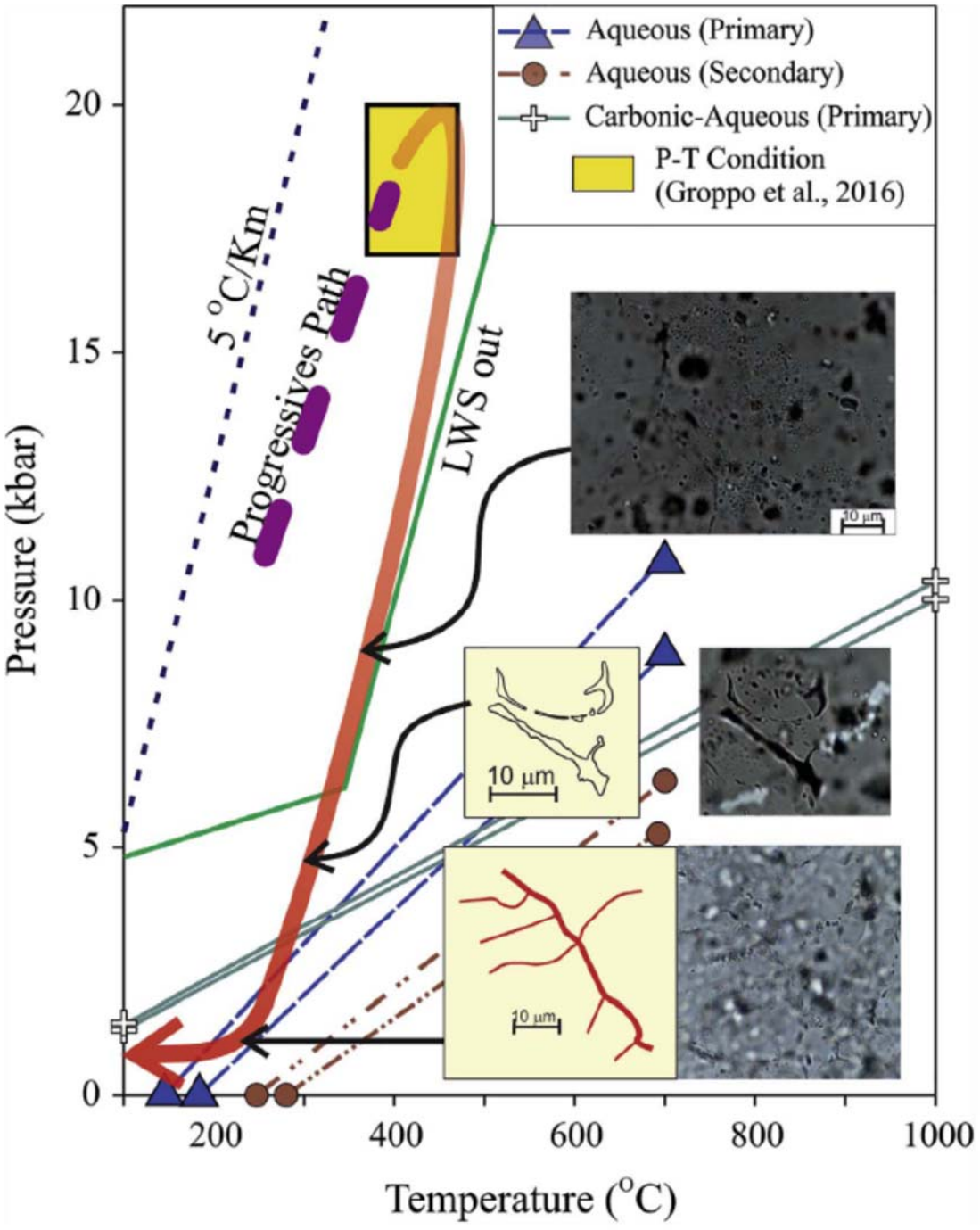
Aqueous (Primary)
Aqueous (Secondary)
Carbonic-Aqueous (Primary)
P-T Condition
(Groppo et al., 2016)
5 °C/Km
Progressives Path
LWS out
10 µm
10 µm
10 µm
Pressure (kbar)
Temperature (°C)
0
5
10
15
20
200
400
600
800
1000

631

632 Fig.8